J. Fluid Mech. (1981), *vol.* 107, *pp.* 465–485
Printed in Great Britain

The dispersion of short wavelets in the presence of a dominant long wave

By O. M. PHILLIPS

Department of Earth and Planetary Sciences, The Johns Hopkins University, Baltimore, Maryland 21218

(Received 21 April 1980 and in revised form 16 September 1980)

The characteristics are studied of short surface waves superimposed upon, and interacting with, a long, finite-amplitude dominant wave of frequency N. An asymptotic analysis allows the numerical investigation of Longuet-Higgins (1978) to be extended to higher superharmonic perturbations, and it is found that, although they are distorted by the underlying finite-amplitude wave, gravity wavelets continue to propagate freely provided the dominant wave does not break. Capillary waves can, however, be blocked by short, steep, non-breaking gravity waves, so that in a wind-wave tank at short fetch and high wind speed, freely travelling gravity–capillary waves can be erased by the successive dominant wave crests.

A train or group of short gravity waves suffers modulations δk in its local wavenumber because of the straining of the long wave, and *large* modulations $C\delta k$ in its apparent frequency measured at a fixed point (where C is the *long* wave phase speed), largely because of the Doppler shifting produced by the dominant wave orbital velocity. The spectral signatures of a wave train are calculated by stationary phase and are found to have maxima at the upper wavenumber or frequency in the range. If an ensemble of short-wave groups is sampled at a given frequency f at a fixed point, the signal is derived from groups with a range of intrinsic frequencies σ, but is dominated by those at the long-wave crest for which $f = \sigma + \mathbf{k}.\mathbf{u}_0$, where u_0 is the orbital velocity of the dominant wave. The apparent phase speed measured by a pair of such probes is the sum of the propagation speed c of the wavelet and the orbital velocity u_0 of the long wave. When f/N is large, the apparent phase speed approaches u_0, independent of f. These results are consistent with measurements by Ramamonjiarisoa & Giovanangeli (1978) and others in which the apparent phase speed at high frequencies is found to be independent of the frequency – the measurements do not therefore imply a lack of dispersion of short gravity waves on the ocean surface.

1. Introduction

Recently, there have been several sets of measurements seeking to determine, as a function of frequency, the phase velocity of the shorter components of a field of wind-generated waves. One method, apparently the most direct, involves measuring the surface displacement at two points separated by a distance Δx in the wind direction, filtering the two signals at a fixed frequency f and finding the time delay Δt required for maximum correlation. The phase speed c at this frequency f is then taken as $\Delta x/\Delta t$. Measurements of this kind have been made in laboratory wind-wave tanks

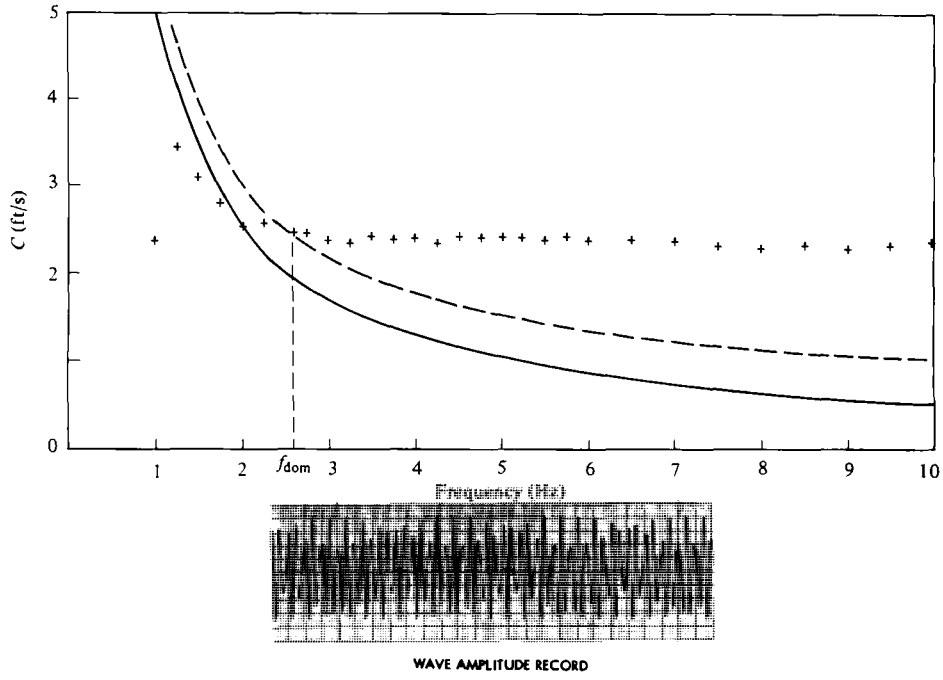

FIGURE 1. Apparent phase speeds of frequency components of wind waves measured by Lake & Yuen (1978) at a fetch of 30 ft and a mean wind speed of 35 ft s^{-1}. f_{dom} represents the frequency of the spectral peak; the solid curve is the linear dispersion relation, and the broken curve is this dispersion relation with an added 'wind drift contribution' of 0·51 ft s^{-1} independent of frequency.

by Ramamonjiarisoa (1974; see also Ramamonjiarisoa & Coantic (1976)) and by Lake & Yuen (1978); they have yielded the striking result shown in figure 1 that the apparent phase speed of wave components with frequencies higher than that of the spectral peak is very nearly *independent of the frequency*. The gravity waves seem to be non-dispersive! The same kind of measurement in the field, made by Ramamonjiarisoa & Giovanangeli (1978) and summarized in figure 2, suggests that here also the phase velocity of short wavelets becomes independent of frequency but now only for frequencies beyond some multiple of that of the spectral peak.

These results are indeed very curious and quite inconsistent with the linear dispersion relation $c = g/\sigma$ for short gravity waves. Ramanonjiarisoa (1974) has considered the effects of both a finite angular spread of the short waves and a wind-induced mean drift near the surface, but neither alone nor the two in combination is capable of reconciling the measurements with linear theory. To add to the confusion, Doppler radar measurements by Plant & Wright (1979) give no hint of this effect. Though covering only a rather small frequency range (2·6 to 4·8 Hz, with a spectral peak at 3·3 Hz), their measurements under conditions similar to those of Lake & Yuen gave phase speeds consistent with the usual dispersion relation after allowance for the wind-induced mean surface drift. More recent measurements by Huang *et al.* (1980) of the simultaneous slope and time derivative of the surface displacement also agree with the classical dispersion relation, though the propagation of harmonics of the basic wave at its phase speed is also observed.

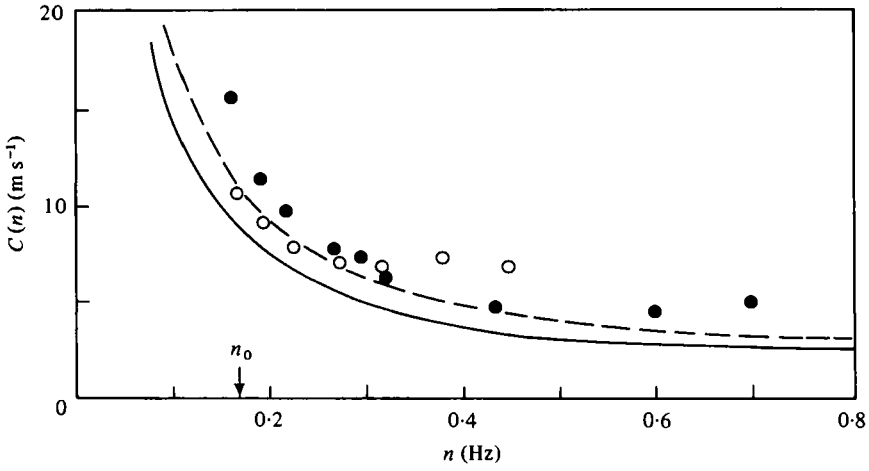

FIGURE 2. Measurements by Ramamonjiarisoa & Giovanangeli (1978) under two different field conditions. The solid curve again represents the linear dispersion relation; the broken curve includes a correction for angular spread of the waves, proportional to $\cos^2\theta$. ○, $U_{26} = 8$ m s^{-1}; ●, $U_{26} = 10$–13 m s^{-1}. $\Delta X = 3$ m.

Nevertheless, so clear were the results shown in figure 1 that Lake & Yuen (1978) were led to propose that 'a non-linear wind–wave system can be completely characterised, to a good first approximation, by a single non-linear wave train having a carrier frequency equal to that of the dominant frequency in the wind-wave spectrum... the spectral components (being) bound wave components of a single dominant wave and... not a random collection of free waves, each of which obeys the usual dispersion relation'. Though figure 1, taken at face value, certainly suggests this proposition, the dynamical reasons for it are obscure. If it is true, why are short, free waves suppressed, or unable to exist, or perhaps unable to be generated by the wind in the presence of a relatively steep, longer dominant wave? If it is false, how does one account for the measurements of figures 1 and 2? The matter is clearly a basic one that demands resolution.

A convenient starting point for the enquiry is provided by the precise numerical calculations of Longuet-Higgins (1978) on the superharmonic perturbations of finite-amplitude gravity waves. This work was based upon a general analytical and numerical method developed by Longuet-Higgins & Cokelet (1976) for calculating the deformation of the free surface under gravity of a two-dimensional irrotational motion that is time dependent and periodic in the horizontal co-ordinate. No restrictions on slope are involved. In his 1978 study, Longuet-Higgins investigated the normal mode perturbations of a finite-amplitude gravity wave for scales that are smaller than that of the basic wave; in particular, those having an integral number of waves in this interval. When the steepness of the fundamental is small, the normal modes simply assume the form of freely travelling waves distorted slightly by the basic wave. As the steepness increases, the frequency of each normal mode perturbation decreases somewhat as shown in figure 3, but the modification is slight. Note that, in figure 3, the frequencies σ are observed in a frame of reference moving with the basic wave, that in this figure n is the mode number (the number of perturbation wavelengths in the basic wavelength) and that negative values of n specify waves moving in the opposite direction. The eigen-

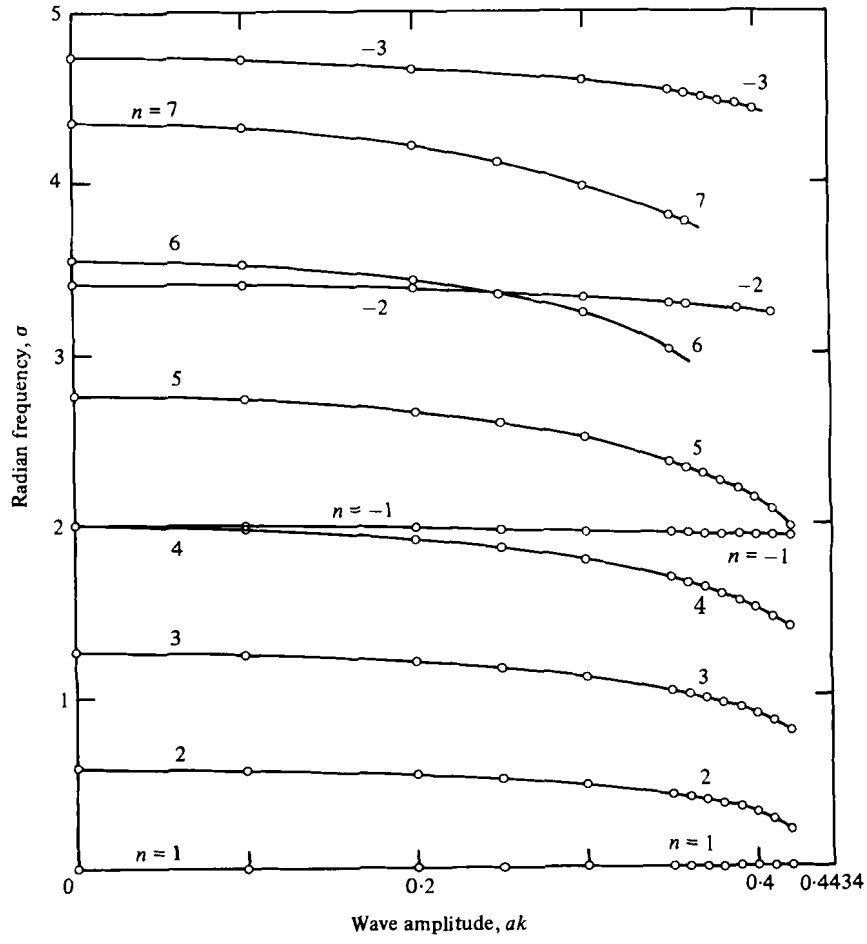

FIGURE 3. Calculations by Longuet-Higgins (1978) on the frequencies of normal mode perturbations to a finite-amplitude gravity wave as functions of the dimensionless amplitude ak of the unperturbed wave.

functions for the various modes are shown in figure 4. For relatively large positive n, the disturbance amplitudes are greatest at the crests and the local wavelength there is least. Even for a basic wave slope as extreme as 0·4 (steep laboratory wind-generated waves have slopes only in the range 0·2–0·3), there is no hint of the non-existence of travelling normal modes or of their phase velocity approaching that of the fundamental ($\sigma \to 0$) in this frame of reference. These results then offer no support to the contention of Lake & Yuen that finite-amplitude wave systems in the ocean are non-dispersive; the higher modes are travelling waves superimposed on the basic non-linear wave and distorted by it in both magnitude and local wavelength, but still propagating with a characteristic frequency.

There remains the (distant) possibility that even higher modes may show a different behaviour; this will be investigated next using the asymptotic techniques appropriate to short waves interacting with much longer ones. There is also the possibility that capillarity effects of the short waves may have an important influence at least under

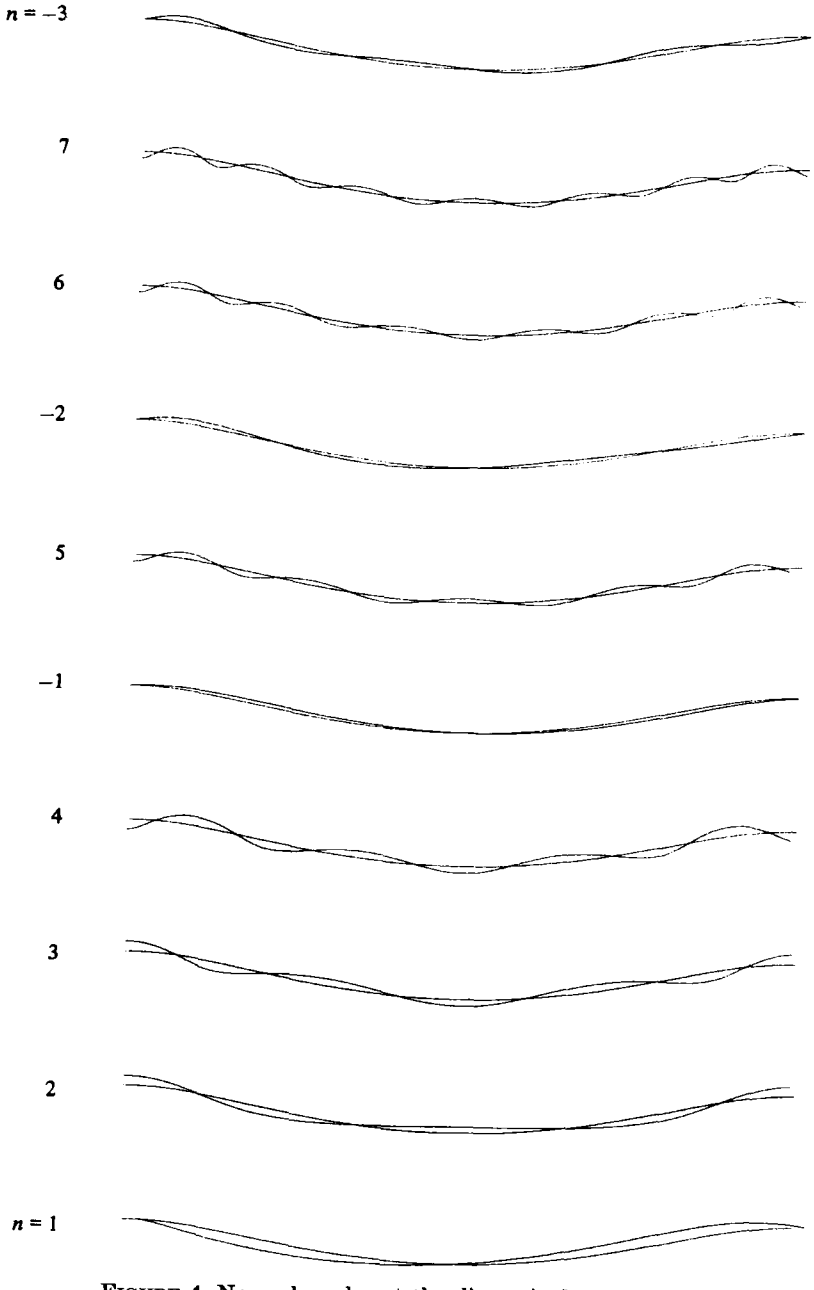

FIGURE 4. Normal modes at the dimensionless amplitude $ak = 0{\cdot}2$ calculated by Longuet-Higgins (1978).

laboratory conditions, when the waves influenced by capillarity may have frequencies only about three times that of the spectral peak. This second possibility will be found to be real and a part of the difference between laboratory and field results shown in figures 1 and 2.

2. Short gravity wave trains on a finite-amplitude long wave

Consider a train of short waves superimposed upon and interacting with a long, steady finite-amplitude wave moving with phase velocity C. In a frame of reference moving with the long wave, the distribution of the tangential surface velocity $u(s)$ associated with the long wave itself is steady and specified by

$$u^2(s) = C^2 - 2g\zeta, \tag{2.1}$$

where ζ is the surface elevation of the basic wave above mean water level. At the long wave crest, the magnitude $u(s)$ is a minimum, decreasing to zero as the Stokes limiting form is approached.

The short waves propagate along this curved moving surface and, if the ratio of long-to-short wavelengths is sufficiently great, the local dispersion relation can be obtained by a simple analysis. In the vicinity of some point P at the surface of the undisturbed wave, let n be the local normal outwards and s the tangential co-ordinate. If the wave perturbation is represented by a displacement $\eta(s,t)$ in the direction of n and the associated velocity perturbation $\mathbf{v}(s,n,t) = \nabla\phi'$, the surface boundary condition of constant pressure is that

$$\frac{\partial\phi'}{\partial t} + \frac{1}{2}\left\{\left(u + \frac{\partial\phi'}{\partial s}\right)^2 + \left(\frac{\partial\phi'}{\partial n}\right)^2\right\} + g(\zeta + \eta\cos\theta) = \text{const.}, \tag{2.2}$$

where θ is the undisturbed surface slope and the condition is applied at $n = \eta$. Now in the second term,

$$u_\eta^2 = u_0^2 + 2u_0\eta\left.\frac{\partial u}{\partial n}\right|_0,$$

correct to the first order, and in terms of the stream function Ψ of the basic flow

$$\frac{\partial u}{\partial n} = \frac{\partial^2\Psi}{\partial n^2} = -\frac{\partial^2\Psi}{\partial s^2} = \frac{1}{2R}\frac{\partial\Psi}{\partial n} = \frac{u}{2R},$$

since s is locally in the direction of $\Psi = \text{const.}$ and where R is the local radius of curvature of the mean surface, a streamline. At the crests, $R < 0$. Consequently, correct to the first order in the short-wave slope, the condition (2.2) becomes

$$\frac{\partial\phi'}{\partial t} + \tfrac{1}{2}u^2 + u\frac{\partial\phi'}{\partial s} + \frac{u^2}{R}\eta + g(\zeta + \eta\cos\theta) = \text{const.},$$

to be applied at the mean free surface, and, after subtraction of (2.1), we have for the short-wave fluctuations

$$\left(\frac{\partial}{\partial t} + u\frac{\partial}{\partial s}\right)\phi' + (g\cos\theta + u^2/R)\,\eta = 0, \tag{2.3}$$

on the surface $n = 0$. Specification of the perturbation motion is completed by the linear kinematic boundary condition at the mean surface

$$\frac{\partial\phi'}{\partial n} = \left(\frac{\partial}{\partial t} + u\frac{\partial}{\partial s}\right)\eta, \tag{2.4}$$

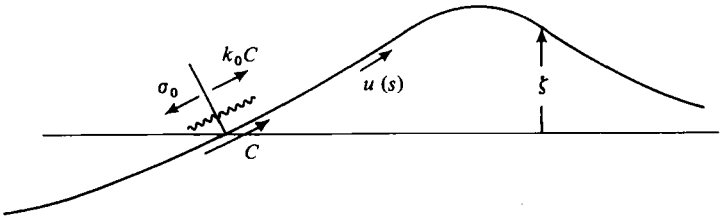

FIGURE 5. Definition sketch.

together with Laplace's equation for ϕ'. These equations are precisely analogous with those for a level mean surface with current u, except that the gravitational acceleration g is replaced by

$$g' = g'(s) = g\cos\theta + u^2/R. \tag{2.5}$$

The effective acceleration due to gravity is then simply the component normal to the undisturbed surface plus the centripetal acceleration. Accordingly, the local intrinsic frequency is

$$\sigma = \{(g\cos\theta + u^2/R)\,k\}^{\frac{1}{2}}, \tag{2.6}$$

where k is the local wavenumber magnitude. The local wave energy density

$$E = (2k)^{-1}\rho\sigma^2a^2, \tag{2.7}$$

where a is the wave amplitude. If capillarity becomes important, then

$$\sigma = (g'k + \gamma k^3)^{\frac{1}{2}}, \tag{2.8}$$

where γ is the surface tension divided by water density.

The distribution of the wavenumber of the short wave with respect to phase of the long wave is specified by the kinematic conservation equation

$$\partial\mathbf{k}/\partial t + \nabla(\sigma + \mathbf{k}.\mathbf{u}) = 0,$$

together with (2.6) for pure gravity waves or (2.8) if capillarity is important. Since in figure 5 the short-wave pattern is steady relative to the long-wave profile, the frequency of short waves passing a given phase point on the long waves is constant:

$$-\sigma + ku(s)\cos\alpha = n_0 = -\sigma_0 + k_0C\cos\alpha_0, \tag{2.9}$$

where α is the angle between the local wavenumber and $u(s)$ (in the plane of figure 5) and the suffix zero specifies properties of the short waves at the point where $\zeta = 0$ and $u(s) = C$. Further, since the short-wave pattern is independent of y (perpendicular to the plane of figure 5), and $\nabla\times\mathbf{k} = 0$,

$$k_y = \text{const.} = k\sin\alpha = k_0\sin\alpha_0.$$

Consequently from (2.9),

$$-\sigma + \{k^2 - k_0^2\sin^2\alpha_0\}^{\frac{1}{2}}\,u(s) = n_0. \tag{2.10}$$

It is easy to see from (2.9) that the only short waves with $n_0 = 0$ (so that the velocity of points of constant phase in the plane of figure 5 is equal to C) are those highly oblique to the basic wave. For, if $n_0 = 0$:

$$\cos^2\alpha_0 = \frac{\sigma_0^2}{k_0^2C^2} = \frac{(g_0'/k_0)}{C^2} \leqslant \frac{g_0'}{g}\frac{K}{k_0} \leqslant \frac{K}{k_0} \ll 1,$$

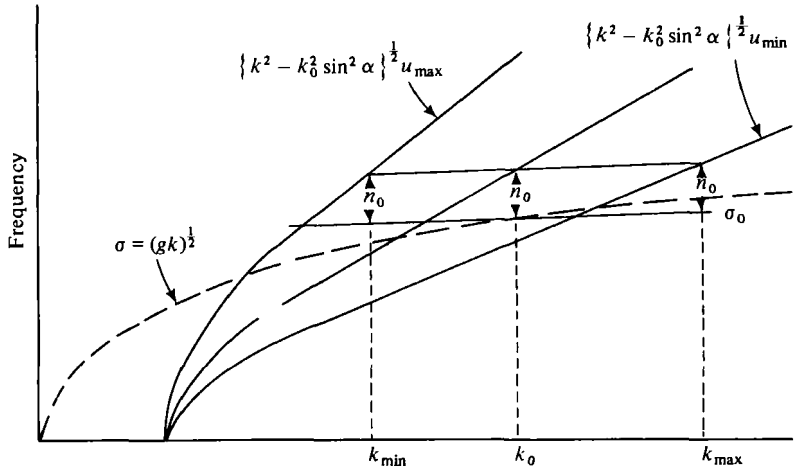

FIGURE 6. A geometrical construction illustrating the variations in wavenumber of short gravity waves with respect to phase of a long wave.

where K is the primary wavenumber. All other short-wave components have $n_0 > 0$ and a phase velocity projected on this plane that is less than C.

Simple algebraic expressions can be derived from (2.9) together with the dispersion relation $\sigma = (g'k)^{\frac{1}{2}}$ for the distributions of local wavenumber, intrinsic frequency, etc., in the case $\alpha = 0$ corresponding to Longuet-Higgins' (1978) calculations. The substitution $k = \sigma^2/g'$ in (2.9) when $\alpha = 0$ gives a quadratic equation for $\sigma(s)$ in terms of $u(s)$ and $g'(s)$, whence

$$\frac{\sigma(s)}{\sigma_0} = \frac{g(s)}{2\beta f(s)}\left\{\left[1 + \frac{4\beta(\beta-1)f(s)}{g(s)}\right]^{\frac{1}{2}} + 1\right\}, \tag{2.11}$$

where $g(s) = g'(s)/g_0$, $f(s) = u(s)/C$ and $\beta = C/c_0 \gg 1$.
The distribution of local wavenumber is

$$k(s)/k_0 = [g(s)]^{-1}(\sigma(s)/\sigma_0)^2. \tag{2.12}$$

The distribution of short-wave energy density is specified by the action conservation law – in a frame of reference moving with the long waves, the action density is independent of time and the flux of action is constant. Thus

$$[u(s) - c_g(s)]\,E/\sigma = \text{const.} = (C - \tfrac{1}{2}c_0)\,E_0/\sigma_0,$$

whence

$$E(s)/E_0 = (\beta - \tfrac{1}{2})\{\beta f(s)(\sigma/\sigma_0) - \tfrac{1}{2}g(s)\}^{-1}(\sigma/\sigma_0)^2, \tag{2.13}$$

and, from (2.7), the mean-square short-wave amplitude varies as

$$(a(s)/a_0)^2 = [g(s)]^{-1}E(s)/E_0. \tag{2.14}$$

Detailed numerical values of these ratios for various steepnesses of the fundamental wave can be calculated from the profile shapes. It is sufficient for our present purposes to note that these asymptotic expressions agree well with Longuet-Higgins' (1978) calculations for ratios of long to short wavelength (his n) as small as 4.

When the primary wave has small steepness, AK, $\zeta = A\cos Kx$ and it can be shown simply that f and g both are of the form $(1 - AK\cos Kx)$, correct to the first order, with minima at the crests. The ratio f/g differs from unity only by a quantity of order

$(AK)^2$; consequently the variations in intrinsic frequency of the short wave over the long wave are, from (2.11), also of only second order in the long-wave slope. In contrast, the wavenumber ratio varies as $(1 + AK\cos Kx)$ from (2.12), with a maximum at the crests and a minimum at the troughs; the short-wave energy density ratio varies as $(1 + AK\cos Kx)$ from (2.13) and the mean-square amplitude ratio as $(1 + 2AK\cos Kx)$.

In a long wave of finite amplitude, the modulations in wavenumber of the short wave can be illustrated by the simple geometrical construction shown in figure 6. From equation (2.10) the difference between $(k^2 - k_0^2\sin^2\alpha_0)^{\frac{1}{2}}u(s)$ and σ is constant along the long-wave profile. The intrinsic frequency σ changes little between crest and trough, but at the crest, where u is a minimum, k is a maximum $k_{\max}$. As the steepness of the primary wave increases, the velocity $u_{\min}$ at the crest decreases and so does the *slope* of the lowest solid line in figure 6, so that $k_{\max}$ increases. But provided $u_{\min}$ is not zero (the Stokes limiting form with a sharp crest), k is everywhere defined on the profile and everywhere finite.

The results of this section can be regarded as extending those of Longuet-Higgins (1978) to higher mode number disturbances of a finite-amplitude wave and also the earlier results of Longuet-Higgins & Stewart (1960), limited to long waves of small slope, by removing this restriction. Except when the long wave has a limiting form with a 120° angle at the crest (a highly unstable configuration for other reasons as well), short-wave perturbations, though possibly substantially distorted in amplitude and local wavenumber, still propagate relative to the long-wave profile. Though their coupling with the wind will undoubtedly be modified (in perhaps very interesting ways) by their modulations in amplitude and local wavelengths, there is no reason to suppose that it is destroyed. In short, we are unable to find any dynamical support for the Lake–Yuen proposition, at least where gravity waves are concerned.

3. Capillary wave blockage

At laboratory scales, on the other hand, the situation is often very different. In most wind-wave tanks in which the fetch is limited to 10 or 20 m, the dominant wavelength is frequently in the range 10–30 cm while, at the wind speeds of order 10 m s^{-1} used by Ramamonjiarisoa (1974) and Lake & Yuen (1978) the steepness of the dominant wave is large. The wave system is characterized by the frequent appearance of parasitic capillaries ahead of, and travelling with, the dominant wave crests (Longuet-Higgins 1963; Phillips 1977) and by breaking of a substantial fraction of the dominant wave crests. To the eye, the waves certainly look much less dispersive than are the larger-scale wave systems in the field – 'freely' propagating short components moving more slowly than the dominant waves are difficult to discern if they are present at all. One can often see short waves travelling obliquely to the wind such that points of constant phase move in the wind direction at a speed about equal to that of the dominant wave. To this extent, visual observations are consistent with the measurements of Ramamonjiarisoa and of Lake & Yuen.

Part of the reason for the absence of shorter, slower moving components may be that they are simply destroyed by the frequent breaking regions that sweep across the surface, catching them up. The microscale breaking process induced by surface wind drift (Banner & Philiips 1974) can suppress short-wave components but it is unlikely to be significant in this situation since the wind drift layer itself is disrupted by the

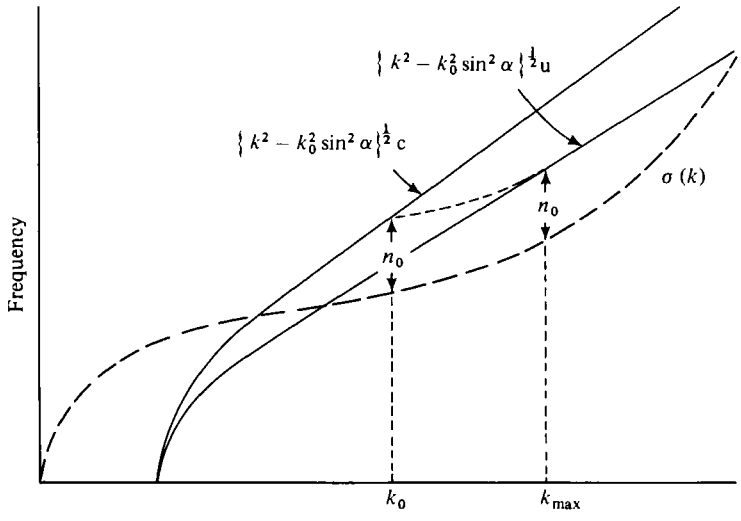

FIGURE 7. The modification of figure 6 to include the effect of capillarity.

frequent breaking events. More important is likely to be a phenomenon of capillary blockage in which, with a dominant wave of sufficient steepness (though not necessarily breaking) short dispersive components are unable to propagate past the dominant wave crest. Any such components that may be generated by the wind are therefore swept up by each long-wave crest.

The kinematics of the process is illustrated in figure 7, a simple modification of figure 6 to include capillarity. In capillary–gravity waves $\sigma \sim k^{\frac{3}{2}}$ when $k \gg (g/\gamma)^{\frac{1}{2}}$. As a group of such waves approaches a crest, $u(s)$ decreases. In figure 7, the asymptotic slope of the solid line is proportional to $u(s)$ and, as the slope decreases, in order to keep the difference n_0 constant, the short wavenumber increases. However, when the slopes of the curves $\sigma(k)$ and $(k^2 - k_0^2 \sin^2\alpha)^{\frac{1}{2}} u(s)$ become equal, the component of the group velocity $\partial\sigma/\partial k$ of the short waves down the face of the long wave just balances the convection up-slope towards the crest. For at this point, when $k = k_m$, say,

$$\begin{aligned} \frac{\partial\sigma}{\partial k} = c_g &= \frac{\partial}{\partial k}\{k^2 - k_0^2 \sin^2\alpha\}^{\frac{1}{2}} u(s) \\ &= \frac{k_m}{(k_m^2 - k_0^2 \sin^2\alpha)^{\frac{1}{2}}} u(s) \\ &= u(s)/\cos\alpha_m, \end{aligned} \tag{3.1}$$

where α_m is the angle between the short waves and the long at this point and since $k_0 \sin\alpha_0 = k_m \sin\alpha_m$. From figure 7, it is clear that if $u(s)$ decreases further (closer to the dominant wave crest) there is no real solution for k. The wave pattern is confined to the region ahead of the blockage point specified by (3.1). In physical terms, the capillary blockage effect occurs because, as the wavenumber of the short wavelets is increased by the long-wave convergence, the group velocity may initially decrease but ultimately it increases again as the wavelength shortens until it is sufficient to overcome the advection towards the long-wave crest.

If the energy density of 'freely propagating' short waves ahead of a capillary blockage point is non-zero, the constancy of action flux

$$(u(s)-c_g\cos\alpha)\,E/\sigma = \text{const.} \tag{3.2}$$

indicates that E becomes indefinitely large as $c_g u(s) - \cos\alpha \to 0$. Possibly in a wind-wave tank, the accumulation of short-wave energy just in advance of a steep primary wave may provide the unsteadiness to provoke breaking.

The wavenumber at the crest of the short component just blocked is such that

$$c_g = \tfrac{3}{2}(\gamma k)^{\frac{1}{2}} = u_{\text{crest}}. \tag{3.3}$$

Longer wavelets will escape blockage. The shortest wave train that can continue to propagate past the crest has, as its wavelength at the crest,

$$\lambda_{\min} = \frac{9\pi\gamma}{2u^2_{\text{crest}}}$$

$$= \frac{9\pi\gamma}{2(C^2-2g\zeta_c)},$$

from (2.1). This can be expressed alternatively in terms of the wavelength Λ of the dominant wave and the ratio of its crest height ζ_c to the maximum height ζ_m of a wave of limiting form with the same wavelength:

$$\lambda_{\min}\Lambda = 9\pi^2(\gamma/g)\,(1-\zeta_c/\zeta_m)^{-1}. \tag{3.4}$$

For example, if $\zeta_c/\zeta_m = 0{\cdot}5$ for a dominant wave with wavelength 10 cm, the shortest freely travelling wave has a length of about 1·5 cm at the crest; if $\Lambda = 1$ m, $\lambda_{\min} = 0{\cdot}15$ cm. Capillary blockage is clearly not a significant field phenomenon, though in laboratory wind-wave tanks, particularly at short fetches, it can significantly restrict the range of 'freely travelling' waves.

This analysis becomes inaccurate when the perturbation wavelength is a significant fraction of that of the basic wave. It would be very interesting to extend Longuet-Higgins' (1978) calculations on super-harmonic perturbations of short gravity waves in which surface tension effects are included. The analysis given here does, however, provide grounds for believing that finite-amplitude wave systems at these scales are indeed much less dispersive than they are at larger scales.

4. The spectral signatures of short-wave trains

A train of short gravity waves interacting with a long wave has an amplitude, a local wavenumber, an intrinsic and apparent frequency, all of which vary with respect to phase of the long wave. How do the usual spectral measures of the waves reflect these variations?

The simplest to calculate is the wavenumber spectrum. In a frame of reference at rest, the short-wave train is

$$\zeta = a(x-Ct)\exp i\chi, \tag{4.1}$$

where the local amplitude $$a = a_0\{E(s)/g(s)\,E_0\}^{\frac{1}{2}} \tag{4.2}$$

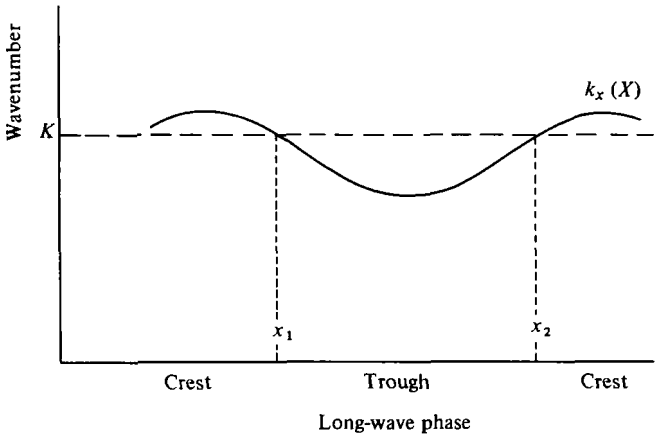

FIGURE 8. The trajectories of local wavenumber with respect to phase of a long wave.

(periodic in x with the long wavelength Λ) is specified as a function of s by (2.14) and (2.12). The distance s along the long-wave profile is, in terms of x,

$$dx/ds = \cos\theta, \tag{4.3}$$

where $\tan\theta$ is the local surface slope. The phase function χ specifies the local wavenumber along the surface $k(s) = \partial\chi/\partial s$ and also in the x, y plane,

$$k_x = \partial\chi/\partial x = k(s)/\cos\theta \quad \text{and} \quad k_y = \partial\chi/\partial y. \tag{4.4}$$

The local wave amplitude a is independent of y and the periodicity in y, k_y, i sunaffected by the long-wave distortion, so that it is sufficient to consider the Fourier representation of (4.1) with respect to k_x. For the sake of simplicity, consider ζ to be periodic in x with wavelength Λ; its Fourier coefficient

$$\begin{aligned}\hat{a}(\kappa) &= \Lambda^{-1}\int_0^\Lambda a(x-Ct)\exp i\chi\exp(-i\kappa x)\,dx,\\ &= \Lambda^{-1}\int_0^\Lambda a(x-Ct)\exp i\phi\,dx,\end{aligned}$$

where $\phi = \chi - \kappa x$. When κ is large, this integral can be evaluated by the method of stationary phase (Lighthill 1978). Significant contributions arise when

$$\partial\phi/\partial x = k_x - \kappa = 0; \tag{4.5}$$

if κ lies between the maximum short wavenumber (at the long-wave crests) and the minimum (in the troughs), there are two phase points x_1, x_2 illustrated in figure 8 satisfying (4.5) with opposite slope of $\partial\phi/\partial x = k_x$, i.e. opposite signs of $\partial^2\phi/\partial x^2$, but with the same amplitude a. Consequently

$$\hat{a}(\kappa) \sim \frac{a(x_1)}{\Lambda}\left[\frac{2\pi}{\partial k_x/\partial x}\right]_{x_1}^{\frac{1}{2}}\{\exp i(\chi_1 - \kappa x_1 + \tfrac{1}{4}\pi) + \exp i(\chi_2 - \kappa x_2 - \tfrac{1}{4}\pi)\}. \tag{4.6}$$

The Fourier coefficient of wavenumber κ then depends, naturally, on the amplitude of the wave train at the phase point where the local wavenumber is equal to κ, and on

the rate at which this local wavenumber varies along the profile. The spectral density $\Psi(\kappa)$ is given by

$$\Psi(\kappa)\,d\kappa = \langle \hat{a}\hat{a}^* \rangle,$$

where $d\kappa = 2\pi/\Lambda$ and the average $\langle\,\rangle$ is over random phases of χ_1, χ_2 for fixed κ (and therefore fixed x_1, x_2). Consequently

$$\Psi(\kappa) = \frac{2\langle aa^* \rangle (x_1)}{\Lambda(\partial k_x/\partial x)_{x_1}}. \tag{4.7}$$

The mean-square surface displacement of the short waves is recovered by integration of (4.7) over κ:

$$\begin{aligned}\overline{\zeta^2} &= \int_{k_{\min}}^{k_{\max}} \Psi(\kappa)\,d\kappa,\\ &= \frac{2}{\Lambda}\int \frac{\langle aa^* \rangle\, d\kappa}{(\partial k_x/\partial x)},\\ &= \frac{2}{\Lambda}\int_0^{\Lambda/2} \langle aa^* \rangle\, dx,\\ &= \overline{\langle aa^* \rangle},\end{aligned}$$

where the overbar indicates the average over the profile of the long waves.

The expression (4.7) becomes inaccurate when the wavenumber corresponds to the maximum at the long-wave crests or to the minimum at the troughs, presenting a singularity, though integrable, at these points. To evaluate the spectral density for these wavenumbers requires the modification to the method of stationary phase appropriate to caustics (Lighthill 1978, pp. 386–91) in which both the first and second derivatives of ϕ vanish. At a crest

$$\hat{a}(\kappa) \sim \frac{2\pi a_c}{\Lambda}[-\tfrac{1}{2}\partial^2 k_x/\partial x^2]_c^{-\frac{1}{3}}\,\mathrm{Ai}\,(z)\exp i(\chi_c - \kappa x_c), \tag{4.8}$$

where

$$z = (\kappa - k_x)[-\tfrac{1}{2}\partial^2 k_x/\partial x^2]^{-\frac{1}{3}}, \tag{4.9}$$

and a_c is the short-wave amplitude at the long-wave crest. A similar expression holds when κ corresponds to the wavenumber at the trough but without the negative sign before $\partial^2 k_x/\partial x^2$, which is positive in the trough. The spectral density near the wavenumber at the long-wave crests is therefore

$$\Psi_c(\kappa) \sim \frac{2\pi\langle aa^* \rangle_c}{\Lambda}[-\tfrac{1}{2}\partial^2 k_x/\partial x^2]^{-\frac{2}{3}}\,\mathrm{Ai}^2(z). \tag{4.10}$$

When the wavenumber κ becomes greater than the maximum wavenumber in the short-wave train at the long-wave crests, $z > 0$ and the Airy function decreases monotonically and exponentially. The singularity in (4.7) when $\partial k_x/\partial x = 0$ at $z = 0$ no longer persists in (4.9) since $\mathrm{Ai}\,(0) = 0{\cdot}355$. The spectral densities at the maximum and minimum wavenumbers are not, however, symmetrical, since, as was shown in §2, $\langle aa^* \rangle_c$ is greater than the corresponding value in the troughs by a factor that increases substantially with the long-wave slope. A wave train, with 'mean' wavenumber k_0 at the points where the long-wave profile intersects mean water level, thus gives a spectral signature in the wavenumber plane as illustrated in figure 9, distributed over a

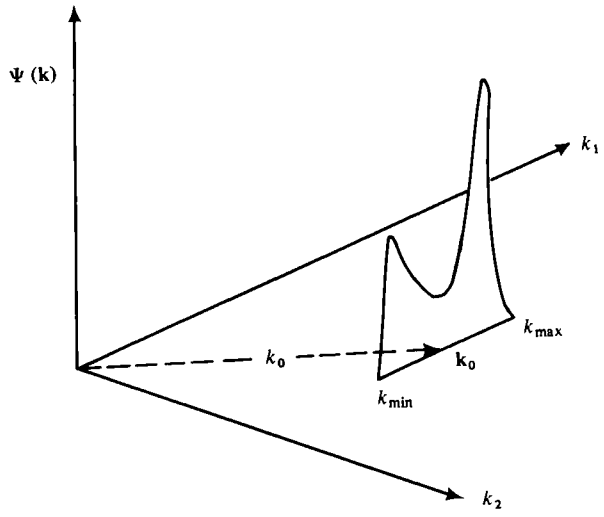

FIGURE 9. The spectral signature on the wavenumber plane of a wave train with mean wavenumber k_0, distorted by a long wave travelling in the 1-direction.

range of wavenumbers in the 1-direction, between k_{max} and k_{min}. Maximum contributions are found at the two ends of the range, the high wavenumber peak being dominant by a factor specified by (2.13)–(2.15).

These calculations have, of course, assumed that the long-wave train is uniform. Under natural conditions, the dominant waves in the ocean are far from uniform and, if short-wave spectra are measured from samples that include many dominant waves, the peaks associated with short-wave trains will be smoothed and distributed over a range determined by the height of the highest individual wave.

The spectral signature in frequency of a group of short waves, measured at a fixed location as the long and short waves move by, is similarly distributed over a range of frequencies, but this time as a result of two effects – the variations in intrinsic frequency σ with respect to phase of the long wave (a second-order modification), together with the 'Doppler effect' associated with the convection of the short waves by the orbital velocities of the long ones. The time derivative of the phase function χ in (4.1) is the apparent frequency

$$-\partial\chi/\partial t = \sigma + k_x u_0, \tag{4.11}$$

where $k_x = k(s)\cos\alpha/\cos\theta$ and u_0 is the horizontal component of the long-wave orbital velocity at the surface measured at a fixed reference point as the waves go by. The quantities σ, k_x and u_0 are all functions of $x - Ct$. In terms of $u(s)$, $u_0 = C - u(s)\cos\theta$ so that

$$\begin{aligned} -\partial\chi/\partial t &= \sigma + \frac{k(s)\cos\alpha}{\cos\theta}(C - u(s)\cos\theta), \\ &= \sigma - k(s)u(s)\cos\alpha + k_x C, \\ &= -n_0 + k_x C, \end{aligned} \tag{4.12}$$

from (2.8). At first sight, this last expression is rather surprising. Since n_0 and C are constant, it asserts that the *variations* in apparent frequency are the same *as if* the short wave with a varying wavenumber were moving with the speed C of the *long* wave.

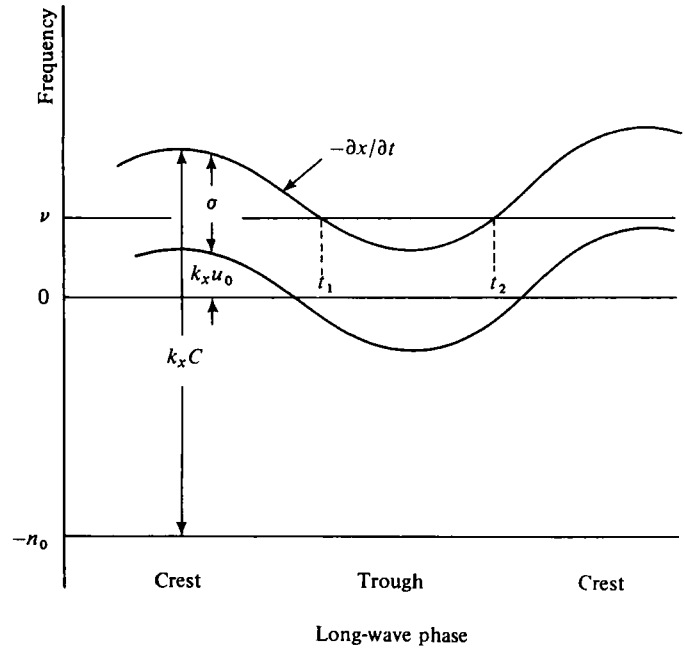

FIGURE 10. The frequency trajectory of short waves superimposed on long.

The correctness of the result is, however, evident. The apparent frequency n_0 is constant in the frame of reference moving with speed C and the last term in (4.12) is simply the Doppler shift modification associated with the change of reference frame, as illustrated in figure 10.

The Fourier component of the surface displacement at a certain frequency ν is

$$\begin{aligned}\hat{a}(\nu) &= T^{-1}\int_0^T \zeta(x,t)e^{i\nu t}dt,\\ &= T^{-1}\int_0^T a(x-Ct)e^{i\phi}dt,\end{aligned} \tag{4.13}$$

where T is the long-wave period and $\phi = \chi + \nu t$. As before, when ν is large, the integral can be evaluated by stationary phase. When ν lies between the maximum and minimum of the apparent frequency $-\partial\chi/\partial t$,

$$\hat{a}(\nu) \sim \frac{a(t_1)}{T}\left[\frac{2\pi}{C^2\,\partial k_x/\partial x}\right]^{\frac{1}{2}}\{\exp i(\chi_1 + \nu t_1 + \tfrac{1}{4}\pi) + \exp i(\chi_2 + \nu t_2 - \tfrac{1}{4}\pi)\}, \tag{4.14}$$

since $-\partial^2\chi/\partial t^2 = C\,\partial k_x/\partial t = C^2\,\partial k_x/\partial x$ from (4.12), k_x being a function of $x - Ct$. The instants t_1 and t_2 are the points of stationary phase, when ν is equal to the apparent frequency of the short-wave group; at these instants $\chi = \chi_1, \chi_2$ respectively. The spectral density $\Phi(\nu)$ is such that

$$\Phi(\nu)d\nu = \langle \hat{a}\hat{a}^* \rangle,$$

where $d\nu = 2\pi/T$, so that

$$\Phi(\nu) = \frac{2\langle aa^* \rangle(t_1)}{C\Lambda(\partial k_x/\partial x)_{t_1}} \tag{4.15}$$

since $\Lambda = CT$. A comparison between this result and (4.7) shows that

$$\Psi(\kappa) = C\Phi(\nu) \tag{4.16}$$

when $\nu = \kappa C - n_0$.

The spectral density of the signature of the short waves is greatest at the apparent frequency found at the long-wave crest since here $\langle aa^* \rangle$ is a maximum while

$$\partial k_x/\partial x \to 0.$$

Near this frequency, a stationary phase calculation similar to that leading to (4.8) gives

$$\hat{a}(\nu) \sim \frac{2\pi a_c}{T}[\phi''']_c^{-\frac{1}{3}} \operatorname{Ai}\left(\frac{\phi_c'}{[\frac{1}{2}\phi_c''']^{\frac{1}{3}}}\right) \exp i\phi_c, \tag{4.17}$$

where

$$\phi = \chi - \nu t,$$

$$\phi' = n_0 - kC - \nu,$$

$$\phi'' = -C\,\partial k/\partial t = -C^2\,\partial k/\partial x,$$

$$\phi''' = -C\,\partial^2 k/\partial t^2 = -C^3\,\partial^2 k/\partial x^2,$$

since $k = k(x - Ct)$. Both ϕ' and ϕ'' vanish at the crest. The spectral density near this frequency

$$\Phi(\nu) = \frac{2\pi\langle aa^* \rangle_c}{C\Lambda}\left[\frac{1}{2}\frac{\partial^2 k}{\partial z^2}\right]^{-\frac{2}{3}} \operatorname{Ai}^2(\phi'/[\tfrac{1}{2}\phi_c''']^{\frac{1}{3}}). \tag{4.18}$$

Comparison with (4.10) shows that the simple relation (4.16) continues to hold. The spectral signature of the wave train is thus distributed over a range of frequencies $(\Delta k)\,C$, where Δk is the difference between the maximum wavenumber at the crest and the minimum in the trough and C is the long-wave speed. Note that, if $C\Delta k$ is sufficiently large, that is, for sufficiently short wavelets on a given swell, the wavelets may be convected backwards in the troughs of the swell so that the frequency range extends below zero and in a measurement appears to be 'folded back' upon $n > 0$.

When the slope of the dominant wave is small, the range of frequencies swept out by the wavelets can be calculated simply. It was pointed out in §2 that the intrinsic frequency σ varies with respect to phase of the swell by the fraction $(AK)^2$, which we neglect when $AK \ll 1$. From (4.11) the measured frequency at the swell crest is

$$f_c = \sigma + ku_0, \tag{4.19}$$

when $\alpha = 0$, where k is the wavenumber there, or

$$k = \sigma^2/g_c' = (\sigma^2/g)\,(1 + AK).$$

Referred to the frequency N of the swell,

$$\frac{f_c}{N} = \frac{\sigma}{N}\left(1 + \frac{\sigma}{N}AK(1 + AK)\right), \tag{4.20}$$

since $u_0 = AKC = AKg/N$. Note that, although AK is small, $(\sigma/N)^2 \gg 1$ and for high-frequency wavelets $(\sigma/N)AK$ may be of order unity or greater. Similarly, the measured frequency in the swell troughs is

$$\frac{f_t}{N} = \frac{\sigma}{N}\left(1 - \frac{\sigma}{N}AK(1 - AK)\right). \tag{4.21}$$

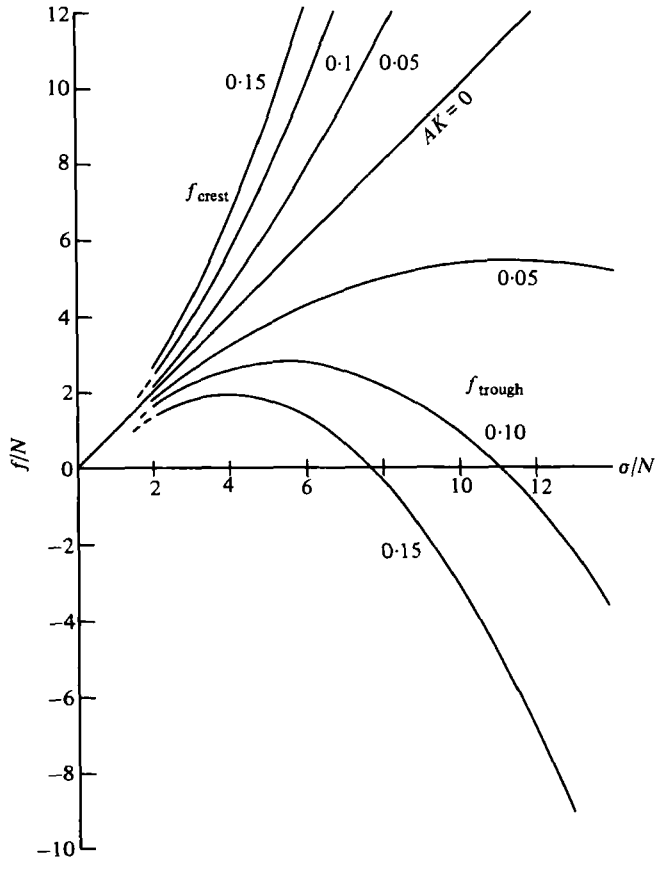

FIGURE 11. Apparent frequencies f, at crest and trough, of wave trains with intrinsic frequency σ for various slopes AK of a long wave or swell with frequency N.

These frequency ranges are illustrated in figure 11 for various small values of AK. For a particular value of σ/N and long-wave slope, the range of apparent frequencies lies between the two curves with the slope indicated – when $\sigma/N = 6$, say, for a swell slope of 0·05, f/N ranges from 4·2 to 7·8. When $\sigma/N > [AK(1-AK)]^{-1}$, the frequency changes sign in the troughs – the short waves are unable to progress forwards against the adverse orbital velocity of the swells and are swept back as the troughs move by.

5. The measurement of 'phase velocity' of short waves by filtered space–time correlations

As described in the introduction to this paper, attempts have been made to measure the phase velocity of short gravity waves by measuring the surface displacement at two neighbouring points, filtering the signals at a given frequency ν and measuring the phase difference, or the time delay for maximum correlation. However, with the modulations in measured frequency of a wave train in the presence of a dominant wave, it is not at all clear that this procedure does in fact measure the phase velocity of the train.

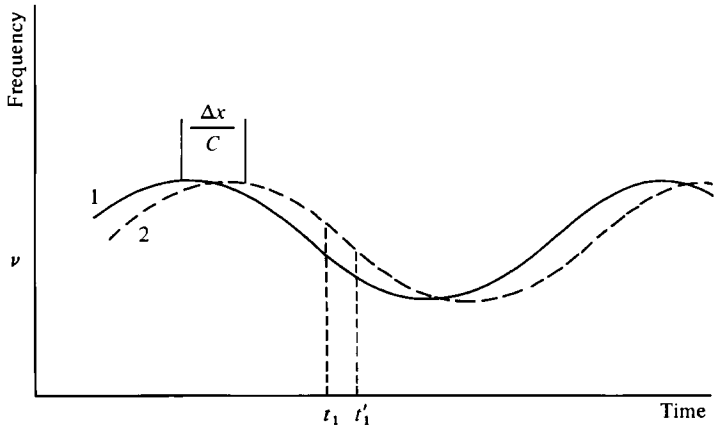

FIGURE 12. Frequency trajectories of a short wave train measured at two neighbouring points.

The field situation generally involves an ensemble of short waves but, for the moment, consider a single train as in the previous sections, with observations at two points separated by a distance Δx. The frequency trajectories in time of the two records are as shown in figure 12, the trajectory for the second measurement position being displaced in time by the amount $\Delta x/C$. For the measurement at point 1, the filtered signal is, from (4.14),

$$\hat{a}(\nu)e^{-i\nu t} = \frac{a(t_1)}{T}\left[\frac{2\pi}{C^2\,\partial k_x/\partial x}\right]^{\frac{1}{2}} \exp i(\chi_1 + \nu t_1 + \tfrac{1}{4}\pi)\exp(-i\nu t), \tag{5.1}$$

together with the contribution from the second crossing. From point 2, the signal is identical in amplitude, but the phase is that appropriate to the instant t_1'. If a time delay τ is introduced into the first signal and it is multiplied by the second, the result is

$$\frac{a_1 a_1^*}{T^2}\left[\frac{2\pi}{C^2\,\partial k_x/\partial x}\right] \exp i[(\chi_1' - \chi_1) + \nu(t_1' - t_1) - \nu\tau]. \tag{5.2}$$

But $\chi' - \chi = k_x\Delta x - n(t_1' - t_1)$ where $n = \nu$, so that the time delay for maximum correlation is indeed $(k_x/\nu)\Delta x$ and the measurement does give the projection of the phase velocity in the direction of Δx in those parts of the long-wave cycle at which the frequency of the wave train is equal to the frequency of filtering.

However, as we have seen, the largest amplitude of the filtered signals occurs when ν corresponds to the wavelet frequency at the long-wave crest, with a secondary maximum at the trough. In the former case, from (4.17), the filtered signal is

$$\hat{a}(\nu)\,e^{-i\nu t} = \frac{2\pi a_c}{T}[\phi'''']_c^{-\frac{1}{3}}\,\mathrm{Ai}\,[\phi'/\tfrac{1}{2}\phi'''']_c^{\frac{1}{3}} \exp i(\phi_c - \nu t). \tag{5.3}$$

If the signal from a neighbouring probe is filtered at the same frequency and a time delay is introduced, the mean product of the two is, as before, a maximum when the time delay is that required for propagation between the two points. At a crest, then, the propagation velocity measured is the *sum* of the orbital speed of the dominant wave and the projection of the intrinsic phase velocity σ/k_x along the line of separation. At the trough, one measures the difference between these two.

Next, suppose that we have groups of short waves with different intrinsic frequencies σ scattered randomly over the dominant wave or swell, and that we examine the characteristics of the short-wave field at a fixed frequency ν. In figure 12, then, for a given long-wave slope, the range of intrinsic frequncies σ/N sampled lies along the horizontal interval between the curves appropriate to that slope. An interesting property of figure 11 is, however, that f/N in the troughs has a maximum of

$$[4AK(1-AK)]^{-1} \quad \text{when} \quad \sigma/N = [2AK(1-AK)]^{-1}$$

from (4.21); at higher intrinsic frequencies than this, the *apparent* frequency reduces. Consequently, if our sampling frequency as a multiple of the dominant wave frequency $\nu/N = f/N > [4AK(1-AK)]^{-1}$, then *there are no contributions from the troughs of the dominant waves by any short-wave train, no matter what the intrinsic frequency.*† For a dominant wave slope as small as 0·1, this already occurs when the sampling frequency is more than 2·8 times the dominant frequency. The principal stationary phase contributions are then derived from the crests of the dominant wave only and the measured propagation speed is the sum of the intrinsic propagation speed σ/k_c and the orbital speed of the swell, or, from (4.19), the apparent phase speed

$$\frac{\nu}{k_c} = \frac{f_c}{k_c} = \frac{\sigma}{k_c} + u_0. \tag{5.4}$$

This can be expressed in terms of ν/N and the dominant wave slope AK. From (4.20),

$$\sigma^{-1} = (2\nu)^{-1}\{1 + [1 + 4AK(1+AK)\nu/N]^{\frac{1}{2}}\}$$

at the crest, and since $g_c' = g(1-AK) = NC(1-AK)$, $u_0 = CAK$, the apparent phase speed of the wavelets is

$$c_{\text{app}} = C(AK + (2\nu/N)^{-1}\{1 + [1 + 4AK(1+AK)\nu/N]^{\frac{1}{2}}\}) \tag{5.5}$$

approaching (from above) a constant, the orbital speed of the long waves, as ν/N increases.

If the slope of the swell is sufficiently small that $[4AK(1-AK)]^{-1} > \nu/N$ (which itself must be greater than about 3 for accuracy of the two-scale analysis) stationary phase secondary maxima at the frequency ν will be detected in the troughs, in fact from wave trains with two different intrinsic frequencies. From (4.21), when AK is small, these are

$$\sigma/N = (2AK)^{-1}\{1 \pm [1 - (4\nu/N)\,AK(1-AK)]^{\frac{1}{2}}\}.$$

If the individual wave groups are saturated at the long-wave crests, their energy density there decreases rapidly with increasing σ (approximately as σ^{-5}); it is further decreased by the straining motion between a saturated crest and an unsaturated trough. It is evident from figure 11 that, when ν/N is rather less than the maximum of f/N for a given slope, the intrinsic frequencies sampled in the troughs are already much greater than the one sampled at the crests, and their relative energy densities insignificant unless AK is very close to zero. Consequently, the expressions (5.4) and (5.5) for the apparent phase speed should continue to hold for observation frequencies somewhat lower than the value $[4AK(1-AK)]^{-1}$ times the dominant wave frequency.

† Except when $f < 0$, corresponding to very short waves (high σ/N) of small amplitude being carried in the opposite direction.

6. Concluding remarks

In the preceding sections, we have shown that there appears to be no dynamical reason why a dominant wave train, short of breaking, should suppress freely propagating gravity waves superimposed upon it. The short waves are distorted and convected by the dominant wave and exchange energy with it, but they continue to propagate at a phase speed that depends upon their own intrinsic frequency and on their location with respect to the dominant wave. As the slope of the dominant wave increases, so does its harmonic content – this of course propagates at the dominant wave speed.

If the record of surface displacement at a point is filtered at a fixed frequency ν significantly above that of the spectral peak, the resulting signal is concentrated at the long-wave crests for three separate reasons. First is the dominance of the stationary phase contribution from these regions. Secondly, the wavelets in an active wind-generated sea are generally locally saturated near the crests, while the divergence in the long-wave flow field may reduce the wavelet amplitude below the saturation limit at other points of the long-wave profile. Thirdly, and probably most important, the wavelets at the crest with apparent frequency ν have the lowest intrinsic frequency σ of all those that appear with apparent frequency ν, and the spectral densities are weighted towards low σ by a factor of approximately σ^{-5}. These three effects in combination provide the expectation that such a filtered signal will exhibit a pronounced 'groupiness' at the long-wave crests that is, in a sense, more apparent than real – much larger, for instance, than the groupiness that would be observed if we could measure at a fixed σ rather than a fixed ν.

The combination of effects also implies that measurement of the phase speed from filtered signals will also be strongly dominated by conditions at the long-wave crests, and the phase speed measured is the sum of the orbital speed of the long waves and the propagation speed at this apparent frequency at the long-wave crest. These results are consistent with the measurements of Ramamonjiarisoa & Giovanangeli (1978) in the field which show at high frequencies an apparent phase speed independent of filtering frequency. The measurements therefore *do not imply* that the short components of a wind-generated wave field are non-dispersive; they are in fact a direct consequence of their dispersive nature combined with their interaction with the longer, dominant waves. They offer no support to the conjecture of Lake & Yuen (1978) described in the introduction.

In laboratory wind-wave tunnels, the situation is accentuated even further. In addition to the measurement bias in favour of the long-wave crests, the relatively short, steep waves generated in these facilities are richer in harmonics that do propagate with the long-wave speed. Under relatively short-fetch, high-wind conditions, many of the wave crests are breaking and this will suppress slower wavelets that may be present. Furthermore, the phenomenon of capillary blockage at very high frequencies suppresses freely travelling capillary–gravity waves even without breaking. These three additional effects imply that the waves generated under such conditions *are* much less dispersive than under most natural conditions in which the slope of the dominant wave is less; the measurement bias implies that filtered space–time correlation measurements will make the waves appear less dispersive still. The striking

measurements of Ramamonjiarisoa shown in figure 1 are then perhaps less surprising than they at first appear.

This work was stimulated by a visit to the Institute de Mécanique Statistique de la Turbulence at Marseille in the spring of 1979 and it is a pleasure to acknowledge the gracious hospitality of the members of the Institute during that time. It was completed in Baltimore with the support of the Office of Naval Research under contract N00014–76–C–0184.

REFERENCES

BANNER, M. L. & PHILLIPS, O. M. 1974 On the incipient breaking of small scale waves. *J. Fluid Mech.* **65**, 647–656.

HUANG, N. E., LONG, S. R., BLIVEN, L. F. & BURNETT, K. 1980 A note on the phase velocities of wave components in a wind wave field. *J. Fluid Mech.* (in press).

LAKE, B. M. & YUEN, H. C. 1978 A new model for nonlinear gravity waves. Part 1. *J. Fluid Mech.* **88**, 33–62.

LIGHTHILL, M. J. 1978 *Waves in Fluids.* Cambridge University Press.

LONGUET-HIGGINS, M. S. 1963 The generation of capillary waves by steep gravity waves. *J. Fluid Mech.* **16**, 138–159.

LONGUET-HIGGINS, M. S. 1978 The instabilities of gravity waves of finite amplitude in deep water. Part 1. Superharmonics. *Proc. Roy. Soc.* A **360**, 471–488.

LONGUET-HIGGINS, M. S. & COKELET, E. D. 1976 The deformation of steep surface waves. 1. A numerical method of computation. *Proc. Roy. Soc.* A **350**, 1–26.

LONGUET-HIGGINS, M. S. & STEWART, R. W. 1960 Changes in the form of short gravity waves on long waves and tidal currents. *J. Fluid Mech.* **8**, 565–583.

PHILLIPS, O. M. 1977 *The Dynamics of the Upper Ocean*, 2nd edn. Cambridge University Press.

PLANT, W. J. & WRIGHT, J. W. 1979 Spectral decomposition of short gravity wave systems. *J. Phys. Oceanogr.* **9**, 621–624.

RAMAMONJIARISOA, A. 1974 Contribution a l'étude de la structure statistique et des mécanismes de génération des vagues de vent. *Inst. Méc. Stat. de la Turbulence, Marseille, Rep.* no. A. O. 10023.

RAMAMONJIARISOA, A. & COANTIC, M. 1976 Loi expérimental de dispersion des vagues produites par le vent sur une faible longueur d'action. *C. R. Acad. Sci. Paris* B **282**, 111–113.

RAMAMONJIARISOA, A. & GIOVANANGELI, J.-P. 1978 Observations de la vitesse de propagation des vagues engendrées par le vent au large. *C. R. Acad. Sci. Paris* B **287**, 133–136.